J. Fluid Mech. (1984), *vol.* 140, *pp.* 175–187
Printed in Great Britain

Mass transport around a horizontal cylinder beneath waves

By JOHN R. CHAPLIN
Department of Civil Engineering, University of Liverpool

(Received 11 August 1983)

Around a horizontal cylinder submerged beneath waves with its axis parallel to the wave crests there exists, owing to streaming flow in the boundary layer, circulation with the same sense of rotation as that of the orbital motion in the waves. Experimental results, for conditions in which the effects of separation are not important, confirm theoretical predictions of the mass-transport velocity at the outer edge of the oscillatory boundary layer. Pressure measurements on the cylinder reveal a nonlinear component which is interpreted as a consequence of circulation induced by steady streaming.

1. Introduction

A striking feature of non-uniform oscillatory flow over a solid surface is the steady 'streaming' that is generated within the boundary layer, but which may extend beyond into the external flow. Being responsible for steady currents in otherwise oscillatory conditions, the streaming flow has been considered mainly in terms of its effects on the kinematics of fluid particles. For example, Schlichting (1932) studied the steady flow patterns around a cylinder oscillating at right-angles to its axis in otherwise-stationary fluid. The boundary layer in this case is of the standing-wave type, in which the oscillations are everywhere in phase. In connection with mass transport near the sea bed beneath waves, Longuet-Higgins (1953) analysed both standing and progressive oscillatory boundary layers. In both cases the velocity distribution of the steady flow across the thickness of the boundary layer is independent of the viscosity, and towards the outer limit of the boundary layer it attains a finite value, which, at least to leading order, is a function only of the local characteristics of the external oscillatory flow. In some contexts (Longuet-Higgins 1960) the width of the steady current in the external flow spreads with time and would ultimately, in the absence of other boundaries, extend to infinity. In other circumstances (Riley 1965; Stuart 1966) the steady current falls to zero across an outer boundary layer whose thickness is finite, but much greater than that of the oscillatory boundary layer.

In work more relevant to the present case, Longuet-Higgins (1970) and Riley (1971) studied the outer flow around a cylinder moving along a circular path without rotation in fluid at rest at infinity. They showed that the oscillatory boundary layer merges into a potential vortex, so that the steady current becomes inversely proportional to the radial distance. Subsequently Riley (1978) considered the case of a cylinder of elliptic cross-section executing the same motion. Owing to the non-uniformity of the streaming flow around the cylinder in this case, it cannot match directly the potential vortex and the necessary transition is provided by an outer boundary layer.

The purpose of this paper is to consider a related case, namely that of the flow around a horizontal cylinder submerged beneath waves of small amplitude with its axis parallel to the wave crests. The characteristics of the oscillatory boundary layer in this example are predominantly those of the progressive type, since the velocity distribution around the cylinder advances one circumference in every wave period. However, the non-uniformity of the ambient flow causes the speed of the steady current at the outer edge of the oscillatory boundary layer to be a function of the angular position around the cylinder, with maximum and minimum values respectively at the top and bottom of the cross-section. Although it is from a different source, the non-uniformity of the streaming flow resembles that around an elliptic cylinder in uniform circular orbital flow (Riley 1978).

The work described in this paper was originally stimulated by consideration of the characteristics of wave loading on components of maritime structures. To within the usual boundary-layer approximation, there can be no change in pressure across the inner (oscillatory) boundary layer. But modifications to the irrotational flow produced by steady streaming, and the greater thickness of the outer boundary layer (when there is one) give rise to the possibility that the pressure at the cylinder's surface differs significantly from that of the ideal fluid flow solution.

In §2 we determine the steady flow to be expected at the outer limit of the oscillatory boundary layer using Batchelor's (1967) general result for non-uniform oscillatory flows. Measurements of particle motion around the cylinder presented in §3 are in good agreement with these predictions, in terms both of instantaneous particle position and mean drift velocity. In §4 we investigate experimentally the concept that the effects of streaming flow can influence pressure at the surface of the cylinder. Measurements suggest that there is a systematic departure in pressure from the ideal fluid-flow result, distinct from the effects of separation.

2. Streaming flow in the oscillatory boundary layer

In a previous paper (Chaplin 1981) the author investigated characteristics of the irrotational flow around a horizontal cylinder submerged beneath gravity waves with its axis parallel to the wave crests. This problem was studied in a more general form by Dean (1948), Ursell (1950) and Ogilvie (1963), who concerned themselves with the effects on small-amplitude waves of a cylinder that is completely submerged, but close to the free surface. Ogilvie formulated the velocity potential in terms of the solutions of an infinite set of linear simultaneous equations, and derived expressions for the first-order force and the time-independent component of the second-order force on the cylinder. For a more deeply submerged cylinder the effects of the disturbances on the incident waves are diminished and, as Ogilvie noted, the flow around the cylinder ultimately can be approximated by means of Milne-Thomson's (1968) circle theorem. Chaplin (1981) showed that, providing the relative submergence $-Y_0/c$ (see figure 1) is greater than about 5, the circle theorem yields a good approximation for the irrotational flow around the cylinder and the associated forces on it. The present paper is concerned with cases in which this condition is met, and we adopt the circle theorem to provide a description of the irrotational flow around the cylinder.

For incident waves of small amplitude a, period $2\pi/\omega$, wavelength $2\pi/K$ in water of constant depth d, the complex potential is

$$\chi = \frac{\omega a}{K \sinh Kd} \sin(KZ + \mathrm{i}Kd - \omega t), \tag{2.1}$$

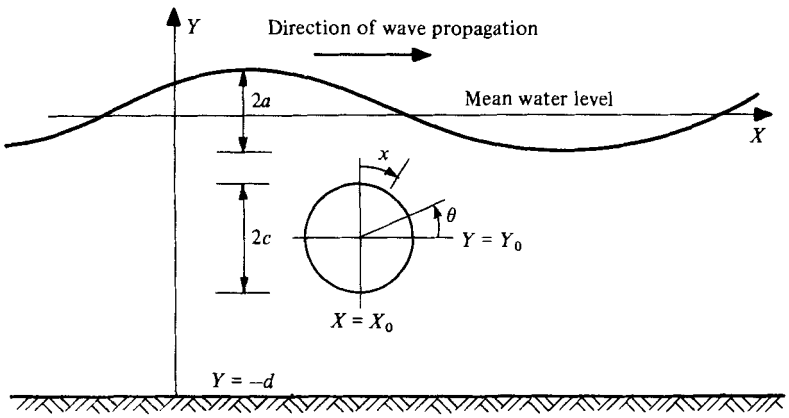

FIGURE 1. Definition sketch.

where $Z = X+\mathrm{i}Y$. At a point on the circle $Z = Z_0+c\,\mathrm{e}^{\mathrm{i}\theta}$, the radial and tangential components of velocity due to the incident waves alone are given by

$$v_r - \mathrm{i}v_\theta = \frac{\omega a}{\sinh Kd}\cos\left(KZ_0 + Kc\,\mathrm{e}^{\mathrm{i}\theta} + \mathrm{i}Kd - \omega t\right)\mathrm{e}^{\mathrm{i}\theta}. \tag{2.2}$$

Using a corollary of the circle theorem, namely that the introduction of the cylinder in the flow causes the radial and tangential velocity components over its surface to be respectively cancelled and doubled, the irrotational flow velocity over the surface of the cylinder may be shown to be equal to the real part of $U\mathrm{e}^{\mathrm{i}\omega t}$, where

$$U = \frac{2\omega a}{\sinh Kd}\mathrm{e}^{-\mathrm{i}Kc\sin kx}\cos\left[kx+\mathrm{i}KS\right], \tag{2.3}$$

in which the velocity is considered positive-clockwise, i.e. having the same direction at the top of the cylinder as that of the wavetrain; x is measured around the cylinder from its uppermost point in the same sense, $k = 1/c$ and $S = Y_0+d+c\cos kx$. In (2.3) the arbitrary phase angle KX_0 has been put to zero.

Similarly, the pressure component at frequency ω at the cylinder's surface derived from the irrotational flow is given by

$$\frac{p_0}{\rho g} = \frac{a}{\cosh Kd}\left[2\cosh\left(KS_0+Kc\cos kx\right)\mathrm{e}^{-\mathrm{i}Kc\sin kx} - \cosh KS_0\right]\mathrm{e}^{\mathrm{i}\omega t}, \tag{2.4}$$

where the real part of any complex quantity is to be understood.

The boundary layer over the surface of the cylinder has periodic progressive characteristics, and must be expected to give rise to a clockwise-streaming flow. Since the magnitude of the velocity fluctuation over the surface of the cylinder is a function of x, the streaming flow must also vary around the circumference. The degree of this non-uniformity reflects that of the incident flow over the diameter of the cylinder, and is therefore determined partly by the value of Kc.

Adopting (2.3) as a description of the external flow over the stationary surface of the cylinder, we proceed to evaluate the streaming flow, neglecting the effects of separation. This will restrict the application of results to small values of the Keulegan–Carpenter numbers K_X and K_Y defined as

$$K_X = \frac{U_0\pi}{\omega c}, \quad K_Y = \frac{V_0\pi}{\omega c}, \tag{2.5}$$

where

$$U_0 = \frac{a\omega \cosh K(Y_0+d)}{\sinh Kd}, \quad V_0 = \frac{a\omega \sinh K(Y_0+d)}{\sinh Kd} \tag{2.6}$$

are the magnitudes of the horizontal and vertical components of velocity in the undisturbed flow at the location of the centre of the cylinder ($K_X \geqslant K_Y$).

For the streaming flow just outside a periodic boundary layer with both progressive and standing components, Batchelor (1967, p. 360) derives the formula

$$\bar{U}_2 = \frac{3}{8\omega}\left[-\frac{\mathrm{d}(UU^*)}{\mathrm{d}x} + \mathrm{i}\left(U^*\frac{\mathrm{d}U}{\mathrm{d}x} - U\frac{\mathrm{d}U^*}{\mathrm{d}x}\right)\right], \tag{2.7}$$

where an asterisk denotes the complex conjugate. $\bar{U}_2$ is the steady Eulerian velocity arising from the non-zero Reynolds stresses within the boundary layer. The second part of the right-hand side of (2.7) arises from the uniform progressive component of the external velocity profile, i.e. that which can be expressed as $A\,\mathrm{e}^{\mathrm{i}(\omega t - kx)}$, where A is a constant. The resulting component of the streaming flow is that appropriate for example in the context of the bed boundary layer beneath uniform progressive gravity waves. The effect of non-uniformity in the progressive pattern of the velocity distribution (i.e. when A is a function of x) arises through the first part of (2.7). The streaming-flow velocity profiles through the thickness of the oscillatory boundary layer are given by Longuet-Higgins (1953) for the progressive and standing components. In the case of the horizontal cylinder beneath waves, both are present, as (2.3) demonstrates. It can be shown that for the general case the streaming-flow velocity profile $\bar{u}_2(y)$ is given by

$$\begin{aligned}\bar{u}_2 = \frac{1}{8\omega}\Bigg\{&\frac{\mathrm{d}(UU^*)}{\mathrm{d}x}[\mathrm{e}^{-2\beta y} - 2\beta y\,\mathrm{e}^{-\beta y}(\cos\beta y - \sin\beta y) \\ &+ 2\,\mathrm{e}^{-\beta y}(\cos\beta y + 4\sin\beta y) - 3] \\ &+ \mathrm{i}\left(U^*\frac{\mathrm{d}U}{\mathrm{d}x} - U\frac{\mathrm{d}U^*}{\mathrm{d}x}\right)[\mathrm{e}^{-2\beta y} - 2\beta y\,\mathrm{e}^{-\beta y}(\cos\beta y + \sin\beta y) \\ &- 2\,\mathrm{e}^{-\beta y}(2\cos\beta y - \sin\beta y) + 3]\Bigg\},\end{aligned} \tag{2.8}$$

where $\beta = (\omega/2\nu)^{\frac{1}{2}}$. It is easily seen that, as $\beta y \to \infty$, $\bar{u}_2 \to \bar{U}_2$ (equation 2.7).

Just outside the oscillatory boundary layer, the total particle-drift velocity, comprising $\bar{U}_2$ and the 'Stokes drift', is given by (Batchelor, 1967, equation 5.13.22)

$$\bar{W}_2 = \bar{U}_2 + \frac{\mathrm{i}}{4\omega}\left(U^*\frac{\mathrm{d}U}{\mathrm{d}x} - U\frac{\mathrm{d}U^*}{\mathrm{d}x}\right). \tag{2.9}$$

With U defined in (2.3), the streaming-flow velocity around the cylinder is

$$\begin{aligned}\bar{U}_2 = \frac{3\omega a^2}{2c\sinh^2 Kd}\{&\sinh 2KS + \sin 2kx \\ &+ Kc(\sin kx \sinh 2KS + \cos kx \cosh 2KS + \cos 3kx)\},\end{aligned} \tag{2.10}$$

and the total Lagrangian drift velocity is

$$\bar{W}_2 = \bar{U}_2 + \frac{\omega a^2}{c\sinh^2 Kd}\{\sinh 2KS + Kc(\cos kx \cosh 2KS + \cos 3kx)\}. \tag{2.11}$$

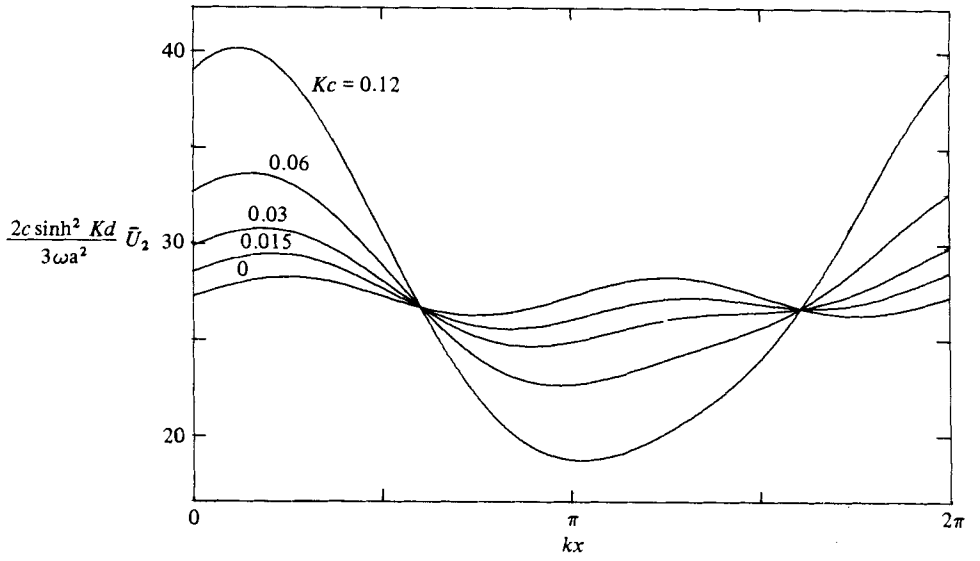

FIGURE 2. Distribution of streaming-flow velocity around the cylinder for $KS_0 = 2$ and various values of Kc.

The distribution of $\bar{U}_2$ around the cylinder is shown in figure 2. It bears a strong resemblance to the distribution of steady streaming calculated by Riley (1978, figure 2) for a cylinder of elliptic cross-section. For small Kc

$$\bar{U}_2 \approx \frac{3\omega a^2}{2c\sinh^2 Kd}(\sinh 2KS_0 + \sin 2kx)$$
$$= \frac{3}{c\omega}[(U_0^2 - V_0^2)\sin kx\cos kx + U_0 V_0]. \tag{2.12}$$

The expression on the right-hand side of (2.12) is identical with the results for $\bar{U}_2$ in the case of a cylinder located in uniform elliptical orbital flow with undisturbed velocity components ($U_0\cos\omega t, -V_0\sin\omega t$). The cases $U_0 = V_0$ and $V_0 = 0$ then refer respectively to the flow around a cylinder forced to move in a fluid at rest at infinity along a circular path (Riley 1971), and around a cylinder oscillating along a straight line perpendicular to its axis (Schlichting 1932). They are moreover equivalent to two special cases of the general uniform flows studied by Longuet-Higgins (1970). The different characteristics of the uniform and non-uniform flows are illustrated in figure 3, which compares particle paths in uniform and wave-induced flows computed by time-stepping the appropriate irrotational-flow solutions.

Just outside the oscillatory boundary layer, the tangential velocity has an unsteady part U (equation 2.3) superimposed on the steady current $\bar{U}_2$ (equation 2.10). When $\bar{U}_2$ exceeds the magnitude of U, there can be no flow reversal. For small Kc this condition arises at all points around the cylinder when

$$a > \frac{2c\sinh Kd}{3\sinh KS_0} \quad \text{approximately,} \tag{2.13}$$

or

$$K_Y > \frac{2\pi}{3} \quad \text{approximately.} \tag{2.14}$$

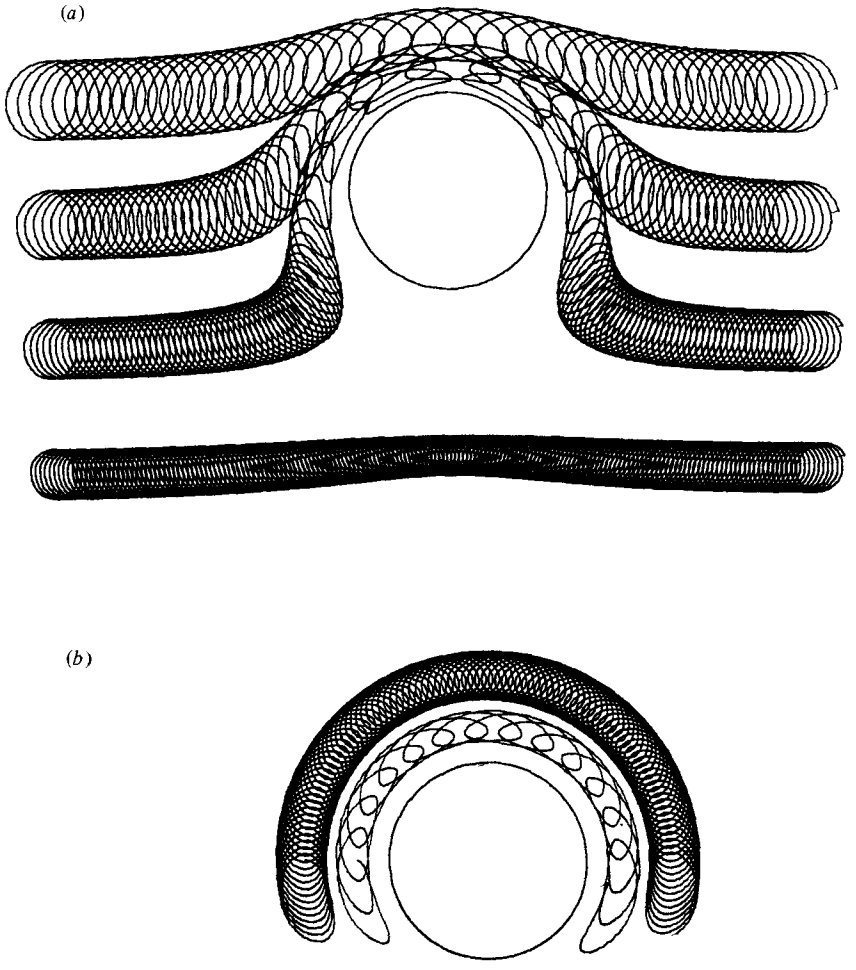

FIGURE 3. Particle trajectories computed from ideal fluid flow analysis: (*a*) for a cylinder in conditions identical to those used in the experiments, with period 1.14 s, amplitude 25 mm; (*b*) for a cylinder in uniform ambient flow with the same undisturbed velocity at the location of the cylinder.

However, for conditions in which this might be expected to occur, the effects of separation may disrupt the assumed flow pattern around the cylinder.

3. Measurements of mean drift velocities

The purpose of the experiments described here was to measure the drift current around the circumference of a horizontal cylinder beneath waves. Measurements were made in regular waves in the 14 m long flume of the Department of Civil Engineering at the University of Liverpool. The width of this flume is 760 mm, and the experiments were carried out with a rigid perspex cylinder of diameter 76 mm spanning the flume at an elevation of 650 mm above the bed. The mean water depth throughout was 850 mm.

The same cylinder was used to provide measurements of pressure in experiments described in §4. It was provided with two pressure tappings at diametrically opposite

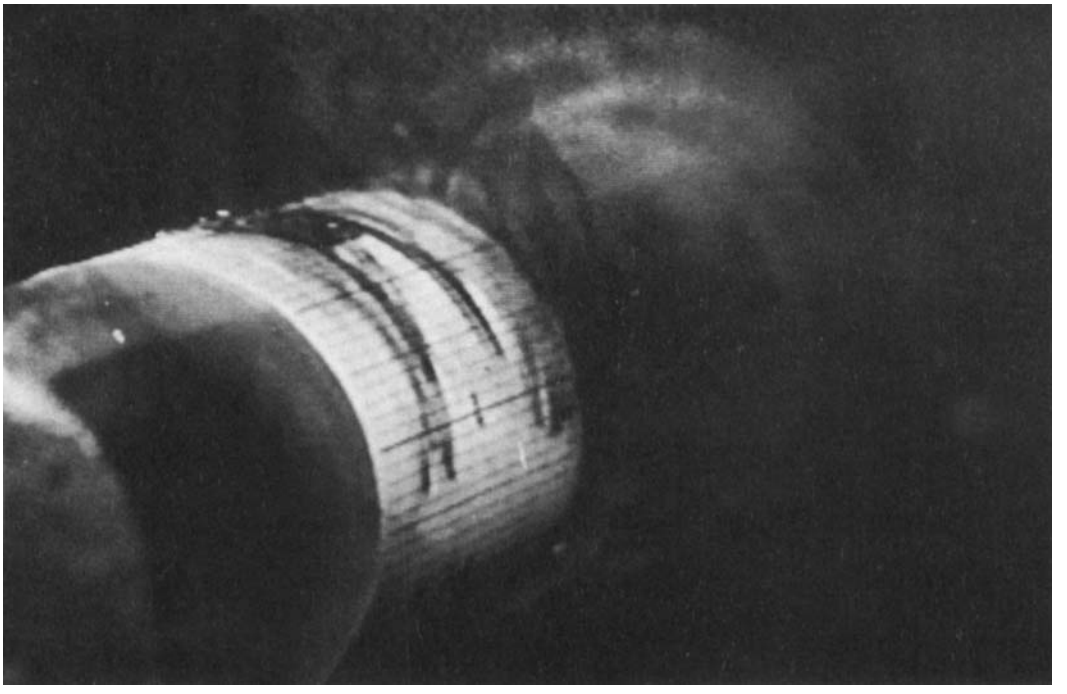

FIGURE 4. Tongues of dye advancing around the cylinder. Also apparent is an indication of the nature of the outer mean flow shown by the dye which has penetrated beyond the oscillatory boundary layer.

points on the central cross-section, and when mounted in the flume could be rotated about its axis to bring the pressure tappings to any desired orientation. The tappings were made from 1 mm stainless-steel tubing, finished flush with the external surface of the cylinder, connecting on the inside with 1 mm internal diameter silicone rubber pipes. Besides being used as pressure tappings, the holes in the cylinder wall, together with the connecting piping, offered a convenient way of introducing dye into and beyond the boundary layer. By means of a small syringe, potassium permanganate solution was forced along one of the pipelines to emerge on the cylinder's surface, then to be swept around the circumference of the cylinder under the action of the Stokes drift and the streaming flow. A piece of graph paper lacquered to the cylinder's surface provided a scale on which the forward movement of the front face of a tongue of dye could be measured. A video recorder with a single-frame advance facility on playback was used to digitize the movement of the dye around the cylinder, at a sampling frequency of 25 Hz. The video records (from which figure 4 is taken) show clearly the front face of the dye. Frame-by-frame analysis revealed quantitatively the steady circulation around the cylinder superimposed on the oscillatory component at the wave frequency.

This method of studying the flow was not suitable for all cases, since in steeper waves the forward velocity of the front face of the dye was sufficient to take it, in only one or two wave periods, more than half the way around the cylinder, and therefore out of the view of the camera. In these circumstances it was not easy to measure reliably the advance of the dye from one wave to the next, and an alternative method was used to find the mean drift velocity. Instead of dye, a saline solution

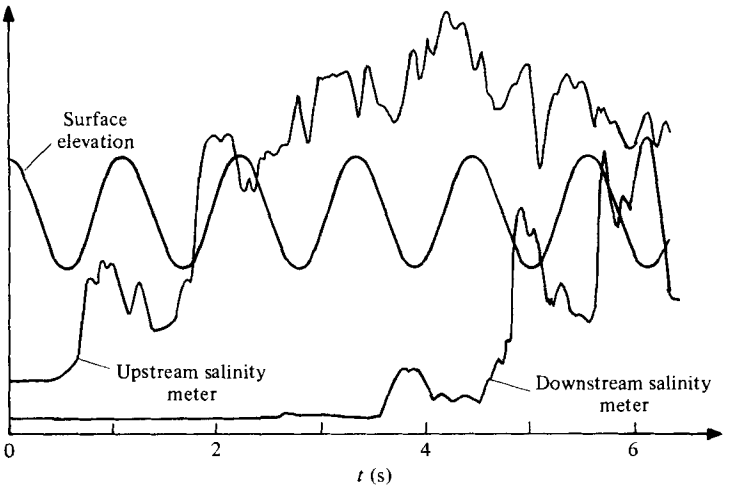

FIGURE 5. Output of salinity meters on the surface of the cylinder showing the time delay corresponding to the mean drift velocity.

was injected into the boundary layer, and its forward progress around the cylinder was detected by means of two pairs of stainless-steel wires, stuck to the surface of the cylinder, lying parallel to its axis. The two wires in each pair were separated by about 5 mm, and the two pairs of wires were positioned 'downstream' of the hole used for introducing the saline solution, by angular separations of 40° and 230° respectively. Changes in resistance between the wires in each pair were detected by means of Churchill monitors normally used for measuring the water surface elevation at a twin-wire resistance wave gauge. In the present application, the arrival of the saline solution over the wires was signalled by a sudden change in the monitor outputs, which were fed to an ultraviolet recorder. A typical record (figure 5) shows the effect of the steady drift component of the flow together with the oscillatory motion at the wave frequency. The mean total drift velocity between the two pairs of wires was computed from the time delay between the two signals, taking into consideration also the different wave phases at which they began. In order to minimize possible errors due to the density difference, the two pairs of wires were positioned symmetrically about the top of the cylinder.

The streaming-flow velocity profile (2.8) has at a finite value of βy (i.e. within the boundary layer) a maximum which in the present circumstances exceeds $\overline{U}_2$ by about 14%. There is a similar, though smaller, percentage overshoot in the Langrangian velocity profile. However, we expect measurements of mean drift velocities to be closer to $\overline{W}_2$, since just outside the boundary layer, where the drift velocity has a more uniform distribution, the concentration of dye or salt is much greater than in the very thin layer of faster-moving fluid inside it.

Figure 6 shows measurements from video recordings of the position of the dye front as a function of time in waves of height 10 mm and period 1.14 s. Also shown for each case is the motion of a particle computed by a time-stepping integration of the oscillatory velocity (equation 2.3), superimposed on the streaming flow (equation 2.10). The agreement, both in terms of the instantaneous and mean motions, is very good. Also shown for reference is the computed mean drift of a particle under the action alone of the streaming flow (equation 2.10), and also under the total mean drift velocity (equation 2.11).

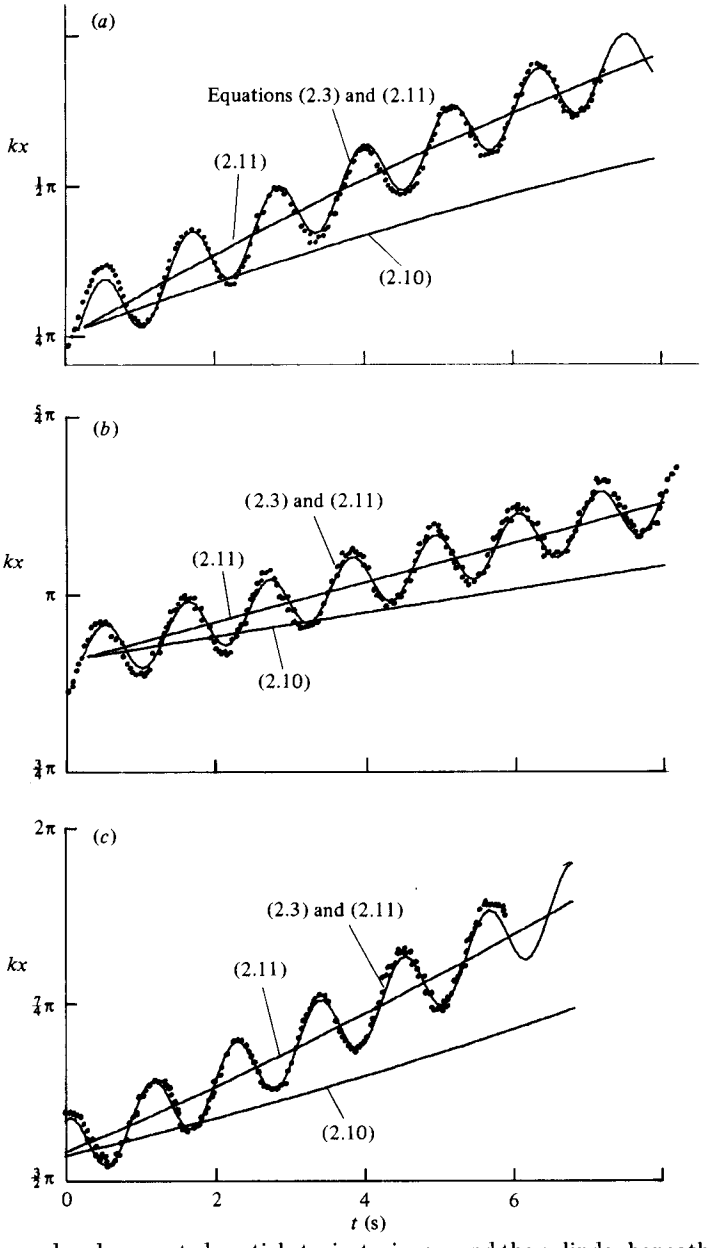

FIGURE 6. Observed and computed particle trajectories around the cylinder beneath waves of period 1.14 s, amplitude 5 mm. Mean particle trajectories derived from (2.11) for the total drift velocity and from (2.10) for the streaming flow alone.

For steeper waves the total mean drift was measured using the salinity meters which provided only the average speed of a particle over an arc of the cylinder's circumference. The results presented below are for the arc $-1.665 \leqslant kx \leqslant 1.665$, and each one is an average of several tests in which the saline solution was introduced at different wave phases. For waves of period 1.14 s and various heights, figure 7 shows the mean drift velocities measured in this way. Also shown for comparison are the

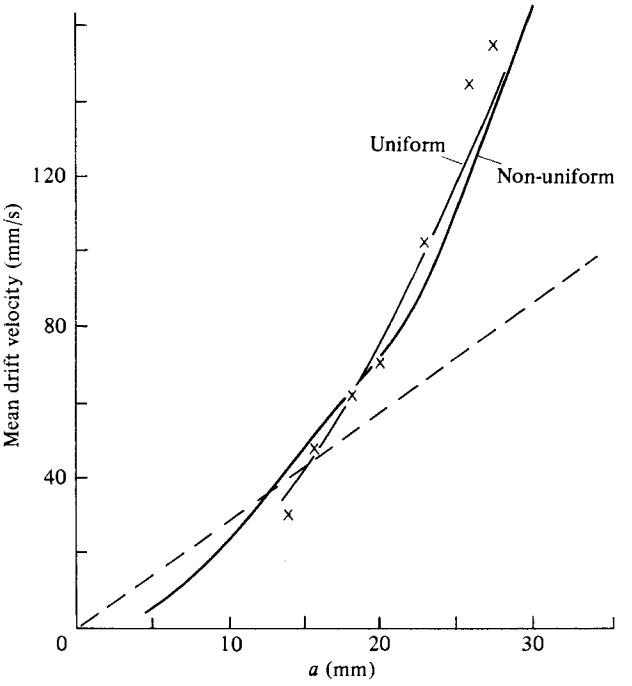

FIGURE 7. Mean drift velocities computed from salinity measurements in waves of period 1.14 s, compared with the results of (2.9) based on wave-induced and uniform ambient-flow conditions. ---, horizontal velocity component of the undisturbed flow.

average drift velocities computed for corresponding conditions from (2.9) on the basis either of uniform elliptical orbital-flow conditions (for which the incident-flow velocities were calculated from linear wave theory) or the non-uniform flow (equation 2.11). As figure 7 shows, the non-uniformity of the flow is not a dominant factor in the mean velocity in these circumstances, and both theoretical lines agree well with the measurements. For the steepest waves used, the mean drift velocity is about twice the incident-flow velocity in the undisturbed waves (shown as a broken line in figure 7). This indicates that the conditions are approaching those in which there is no flow reversal around the cylinder. Although the average results for the steepest waves do not deviate far from the theoretical results, individual measurements for these cases become rather erratic. This was due to the increasing significance of the wave phase at which the saline solution was injected, the difficulty of extracting the mean drift velocity when the time interval between the responses of the salinity meters was less than one wave period, and the increasing effects of separation, observed by means of dye mixed with the saline solution. It is therefore possible that for the steepest waves represented in figure 7, i.e. those with $K_X > 1$, the observed migration of the saline solution at some wave phases was influenced by the fact that it found its way into the wake, which progresses around the cylinder once in every wave period.

4. Measurements of pressure on the cylinder

Pressure measurements on the surface of the cylinder were carried out to test whether a departure from ideal fluid flow results, possibly attributable to the streaming flow, could be identified. For pressure measurements the cylinder was

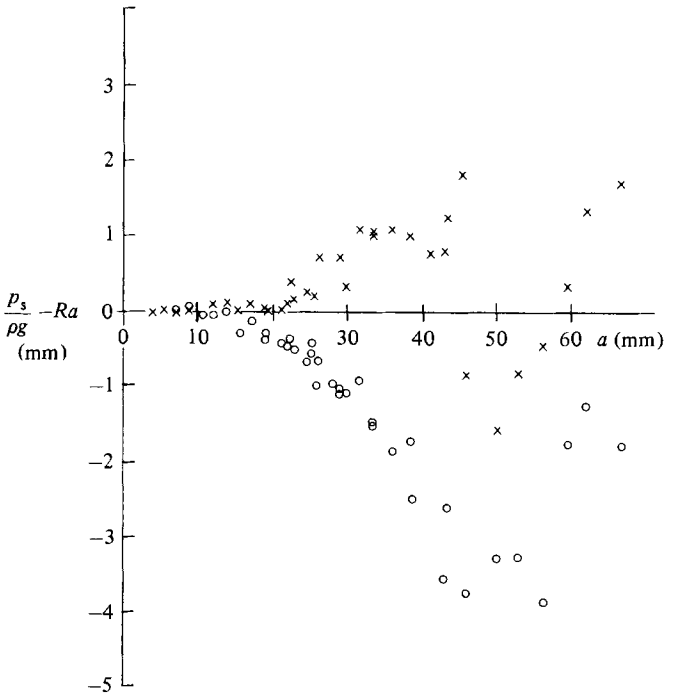

FIGURE 8. Measured deviations in pressure amplitudes from the linear relationship equation (2.4) for waves of various amplitudes, period 1.53 s: ○, $kx = 0$; ×, $kx = \pi$.

mounted as described in §3, and the two pressure tappings were connected to Druck PDCR45 pressure transducers. These were mounted on the inside wall of the flume, just above the highest crest level, in order to minimize the pipe length to the surface tappings, about 60 cm in all. Tests carried out with pipes of length 60 and 120 cm produced indistinguishable results, suggesting that the pressure fluctuations did not suffer serious attenuation due to pipeline losses. The output signals from the pressure transducers and wave gauges were logged at 100 Hz and stored on disk. Results presented below are derived from the components of pressure and surface elevation records at the fundamental wave frequency, extracted by Fourier analysis. In all the tests the cylinder was orientated so that the pressure tappings were exactly at the top and bottom of the cylinder (i.e. at $kx = 0$ and π).

Not surprisingly the amplitude of pressure fluctuations p_s was proportional to the wave amplitude a when a was small. Since we are mainly concerned with deviations in the pressure from this linear relationship, first the pressure response factors $R = p_s/\rho g a$ for the top and bottom of the cylinder were calculated from pressure measurements in small waves. They were found to be in satisfactory agreement with the results of (2.4), based on the measured wave height. For steeper waves, however, the amplitudes of the pressure fluctuations at the top and bottom of the cylinder were respectively initially less and greater than those based on linear theory. Deviations from the linear relationship are shown in figure 8, in which, from experimental results, $p_s/\rho g - Ra$ is plotted as a function of a for waves of period 1.53 s. The source of some scatter in these results lies in the process of resolving small pressure differences, about 1 mm H_2O, from the total fluctuating pressure, which was about 25 mm H_2O for waves of 35 mm amplitude; with proportionately worse signal-to-noise ratios at smaller wave amplitudes.

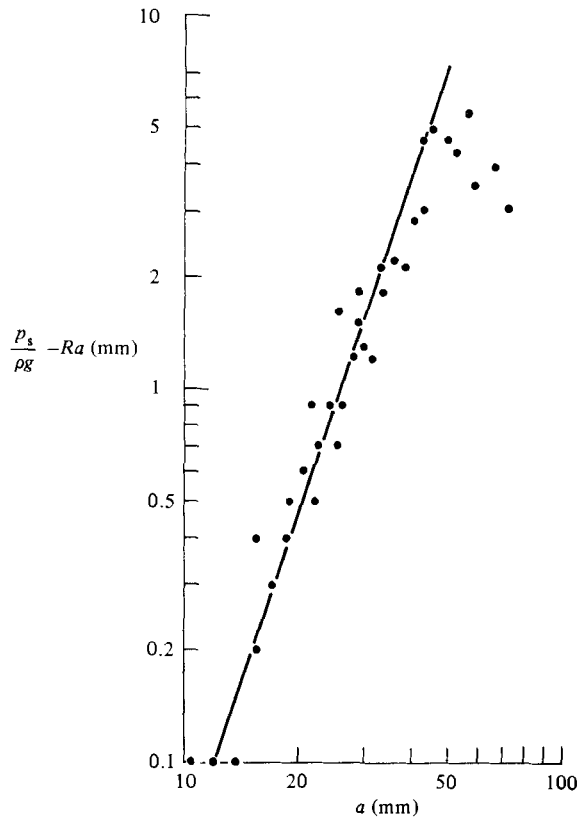

FIGURE 9. Measured deviations in pressure amplitudes at $kx = 0$ from the linear relationship (2.4), for waves of period 1.53 s. ——, best-fit line for measurement with $a < 35$ mm.

For wave amplitudes greater than about 40 mm ($K_X > 2.6$), the large deviations in pressure differences from the trends are indicative of boundary-layer separation from the cylinder. This was also apparent in velocity measurements, which for similar conditions showed evidence of a separated wake close to the cylinder. In figure 9 deviations in pressure amplitudes from the linear relationship are plotted against wave amplitude for the top of the cylinder's cross-section. The least-squares fit to the results for $a < 35$ mm has a slope of 2.97, indicating that the deviation in pressure follows closely the cube of the wave amplitude, up to the point where separation profoundly modifies the flow, introducing more dramatic changes in pressure.

Besides effects of the streaming flow and separation, nonlinear contributions to the pressure at the cylinder are to be expected from the nonlinearity of the free surface boundary condition. Ogilvie's (1963) analysis does not extend to the third order, but it is worth noting that use of the Stokes-series expansion for the description of the incident waves yields for the first nonlinear contribution to the pressure difference across the vertical diameter of the cylinder, at the wave frequency,

$$\frac{\Delta p}{\rho g} = -\frac{K^2 a^3[(5\cosh^4 Kd + \cosh^2 Kd + 3)\sinh KS_0 \sinh Kc + 3\sinh 3KS_0 \sinh 3Kc]}{2\sinh^4 Kd \cosh Kd}. \tag{4.1}$$

This amounts to less than 1 % of the nonlinear pressure difference measured in the experiments.

5. Conclusions

Measurements have been made of the mass transport around a horizontal cylinder submerged beneath waves, with its axis parallel to wave crests. For conditions in which the wave amplitude (or the Keulegan–Carpenter number) is sufficiently small for the effects of separation to be unimportant, and with the cylinder submerged at an elevation about 2.5 diameters below mean water level, the results are in good agreement with predictions. The theoretical analysis was based on the assumptions that the waves were of small amplitude and, at the free surface, were unaffected by the presence of the cylinder.

Pressure measurements on the cylinder can be interpreted as suggesting that modifications to the irrotational flow field, or the existence of an outer boundary layer produced by the streaming flow around the cylinder, make a nonlinear contribution to the force it experiences. Nonlinear pressures observed in the present experiments point to a significant reduction in the inertia force derived from inviscid irrotational flow theory. However, further interpretation of these results must await theoretical developments following on the work of Ogilvie (1963), on nonlinearities at the free surface, and of Riley (1978), on the outer flow associated with the circulation generated by the streaming velocity.

The author is indebted to N. Riley for helpful discussion on the work described in this paper, which was supported by the Science and Engineering Research Council Marine Technology Directorate through the North Western Universities Consortium for Marine Technology. The experiments were carried out with the assistance of Kostas Anastasiou.

REFERENCES

BATCHELOR, G. K. 1967 *An Introduction to Fluid Dynamics.* Cambridge University Press.

CHAPLIN, J. R. 1981 On the irrotational flow around a horizontal cylinder in waves. *Trans. ASME* E: *J. Appl. Mech.* **48**, 689–694.

DEAN, W. R. 1948 On the reflexion of surface waves by a submerged circular cylinder. *Proc. Camb. Phil. Soc.* **44**, 483–491.

LONGUET-HIGGINS, M. S. 1953 Mass transport in water waves. *Phil. Trans. R. Soc. Lond.* A **245**, 535–581.

LONGUET-HIGGINS, M. S. 1960 Mass transport in the boundary layer at a free oscillating surface. *J. Fluid Mech.* **8**, 293–306.

LONGUET-HIGGINS, M. S. 1970 Steady currents induced by oscillations round islands. *J. Fluid Mech.* **42**, 701–720.

MILNE-THOMSON, L. M. 1968 *Theoretical Hydrodynamics*, 4th edn. Macmillan.

OGILVIE, T. F. 1963 First and second order forces on a cylinder submerged under a free surface. *J. Fluid Mech.* **16**, 451–472.

RILEY, N. 1965 Oscillating viscous flows. *Mathematika* **12**, 161–175.

RILEY, N. 1971 Stirring of a viscous fluid. *Z. angew. Math. Phys.* **22**, 645–653.

RILEY, N. 1978 Circular oscillations of a cylinder in a viscous fluid. *Z. angew. Math. Phys.* **29**, 439–449.

SCHLICHTING, H. 1932 Berechnung ebener periodischer Grenzschichtströmungen. *Phys. Z.* **33**, 327–335.

STUART, J. T. 1966 Double boundary layers in oscillatory viscous flow. *J. Fluid Mech.* **24**, 673–687.

URSELL, F. 1950 Surface waves in the presence of a submerged circular cylinder, I and II. *Proc. Camb. Phil. Soc.* **46**, 141–158.